ARTICLES
https://doi.org/10.1038/s41567-022-01642-8
nature physics

Dynamic measurement of gravitational coupling between resonating beams in the hertz regime

Tobias Brack[1,3], Bernhard Zybach[1,3], Fadoua Balabdaoui[2], Stephan Kaufmann[1], Francesco Palmegiano[1], Jean-Claude Tomasina[1], Stefan Blunier[1], Donat Scheiwiller[1], Jonas Fankhauser[1] and Jürg Dual[1] ✉

To date, there have been few dynamic measurements of gravitation in the laboratory, and fully controlled quantitative experiments have been limited to frequencies in the millihertz regime. Here we introduce a fully characterized experiment at frequencies in the hertz regime, which allows a quantitative determination of the dynamic gravitational interaction between two parallel beams vibrating at 42 Hz in bending motion. A large amplitude vibration of the transmitter beam produces a gravitationally induced motion of the high-quality-factor resonant detector beam with amplitudes up to 10^{-11} m. The sub-picometre-resolution measurement is made possible by a setup that combines acoustical, mechanical and electrical isolation; a temperature-stable environment; heterodyne laser interferometry; and lock-in detection. The interaction is quantitatively modelled based on Newton's law of gravitation. Amplitude measurements at varying beam distances follow an inverse square law and agree with theoretical predictions to within approximately three percent. Furthermore, we extract the value of the gravitational constant *G* and near-field gravitational energy flow. We expect our experiment to enable progress in directions where current experimental evidence for dynamic gravitation is limited, such as the dynamic determination of *G*, inverse square law and gravitational shielding.

Gravitation is the weakest of the four fundamental forces of physics. It was first modelled by Newton[1] and then extended with Einstein's theory of general relativity[2]. Experimentally, much progress has been made since Cavendish[3–7]; however, many effects central to gravity have only been measured with a moderate accuracy due to the weakness of the gravitational force. Therefore, $G = 6.6743 \times 10^{-11}\,\mathrm{m^3\,kg^{-1}\,s^{-2}}$ is the fundamental physical constant known to the smallest precision with a relative uncertainty of 22 ppm (ref. [8]). Besides the determination of *G*, recent work has also focused on the investigation of the inverse square law[9–11] and the measurement of gravitational waves at frequencies of around 100 Hz (refs. [12,13]). Measurements in the laboratory have the advantage of having full control over cause and effect without having to wait for something to happen in outer space[14]. Most experiments in this regard have been static or in the millihertz regime[4,6,15]. Although some sources of uncertainty have been resolved, many complications remain, for example, $1/f$ noise or unknown static mass distributions, and the uncertainties are still relatively large[4,5,16]. Also, there are still some differences in recent measurements that are assumed to be systematic errors but remain unexplained. Hence, the only way to give confidence is to measure the same constant using a number of different methods[17]. Although the idea is not new[18,19], dynamic, resonance-based experiments using time-harmonic gravitational fields with frequencies greater than 0.1 Hz are very rare. They start with the observation of an increase in vibrational noise of 20% due to gravitational interaction[20]. Another study used a rotating quadrupole source to dynamically investigate the inverse square law[21]. A rotating body was used to excite the gravitational wave antenna 'EXPLORER' at CERN[22]. More recently, the use of micromechanical oscillators has been proposed to study the inverse square law at small distances[23] or to investigate the theory of quantum gravity using very small source masses[24,25]. None of these experiments, however, showed quantitative agreement between theory and experiment for all gravitational quantities at the same time, and numerous engineering aspects have been mentioned that still need to be resolved[24]. Around 1997, William Walker in our group worked for his doctoral thesis on a dynamic setup consisting of two parallel beams, both vibrating in the vicinity of the first resonant bending mode at a detector resonance frequency of about 40 Hz (ref. [26]). The brass transmitter beam was vibrating with a large amplitude of about 0.01 m in air, generating a dynamic gravitational force field. The tuned detector beam was set into vibration by this force field. The cylindrical detector beam made of quartz glass was placed at a distance of about 0.05 m in a vacuum chamber and had a quality factor (*Q*) of ~210,000. This resulted in a gravitationally induced vibration amplitude of 10^{-9} m of the detector beam. However, because of the high time constant of the detector beam of ~90 min, difficulties in temperature stabilization made it impossible to make precise measurements. Many additional limitations in electronics, optics and disturbing influences (including mechanical and acoustical crosstalk, electromagnetic and magnetic effects, or additional modes of vibration) gave the impression that further work was not promising, and the project was abandoned. Since then, many advances have been made in signal processing, laser interferometry, materials technology, vibration isolation and control theory. The setup was therefore revisited, many improvements were implemented and the setup's limitations were tested. The accomplishments and resulting achievements are presented here. First, the Newtonian theory is applied to the gravitational interaction between two beams to yield a vibrational amplitude. Then, a working setup is described, and the measurement procedure is presented, followed by the quantification of the detector amplitudes for various distances. By comparing the

---

[1]Institute of Mechanical Systems, Department of Mechanical and Process Engineering, ETH Zurich, Zürich, Switzerland. [2]Seminar for Statistics, Department of Mathematics, ETH Zurich, Zürich, Switzerland. [3]These authors contributed equally: Tobias Brack, Bernhard Zybach. ✉e-mail: dual@imes.mavt.ethz.ch

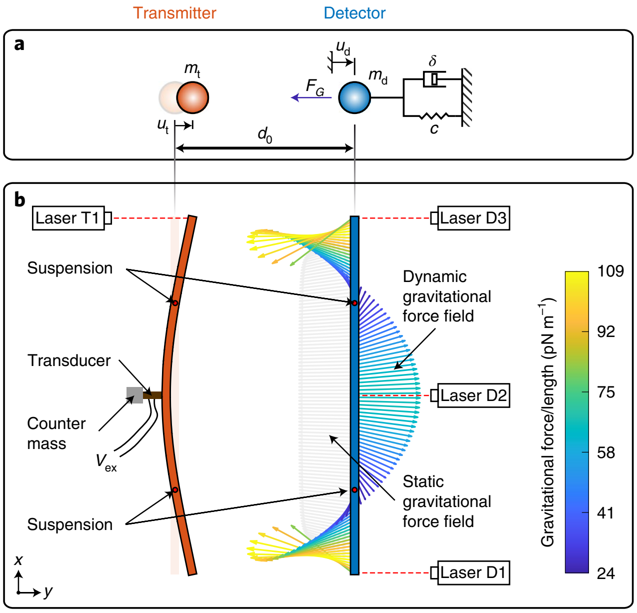

Fig. 1 | Illustration of the measurement principle. a, Simplified SDOF model with transmitter point mass m_t and detector oscillator (point mass m_d, spring constant c and damping constant δ): the transmitter mass, moving with time-harmonic displacement u_t, creates a dynamic gravitational force F_G acting on the detector mass at distance d_0, thus generating an oscillation u_d. When the frequency of excitation matches the resonance frequency of the oscillator, the detector starts to resonate and develops a measurable vibration amplitude. **b**, Sketch of the measurement setup using two bending beams: a transmitter beam (orange), driven by a piezo-transducer with excitation voltage V_{ex}, and a detector beam (blue), both suspended in the nodal points of the first bending mode. The transducer features a countermass to increase the effectivity of excitation. The vibrating transmitter creates a gravitational force field acting on the detector, mainly composed of a static portion (grey colour, qualitatively) and a dynamic portion at the frequency of excitation (coloured). The colour bar quantifies the gravitational force density of the dynamic force field in the x–y plane in pN m^{-1} for the setup presented in this paper ($d_0 = 59$ mm). The motion of both transmitter and detector is measured by laser vibrometers, one for the (large) transmitter motion and three for the (small) detector vibration.

measured amplitudes to the theory, a first estimation of the dynamic gravitational constant G is made based on 18 single measurements, the inverse square law is tested and the gravitational energy flow computed.

Theory of gravitationally coupled oscillators

Figure 1a illustrates two point masses (transmitter mass m_t and detector mass m_d) separated by undisturbed distance d_0. The detector mass is part of a damped spring mass oscillator, characterized by its mass, spring constant c and damping constant δ. When the transmitter mass moves with a time-harmonic displacement $u_t(t) = u_t' e^{i\omega t}$, Newton's law of gravitation yields a dynamic gravitational force acting on both transmitter and detector mass[1].

Due to the varying distance, the force is periodically changing around the static value $F_{G,0} = Gm_d m_t d_0^{-2}$, thus causing the detector mass to vibrate. When the frequency of excitation ω matches the resonance frequency $\omega_0 = (c/m_d)^{1/2}$ of the oscillator, the effect of excitation is maximally amplified, resulting in a displacement of the detector mass that can be approximated by

$$u_d(t) \approx i \frac{2Gm_t Q_d}{d_0^3 \omega_0^2} u_t' e^{i\omega_0 t} \tag{1}$$

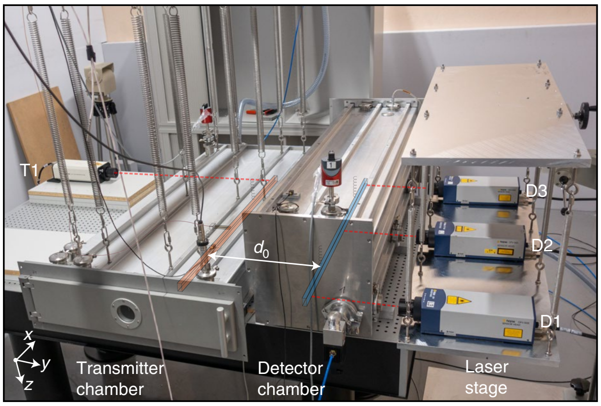

Fig. 2 | Illustration of the measurement setup. The transmitter beam (red drawing), hanging on springs attached at the nodal points of the first bending mode, is located inside the transmitter chamber. The chamber itself is similarly hanging from springs attached to a carrier bar movable in the y direction (not shown). The vibration amplitude of the transmitter is measured using a single-point laser interferometer (T1). The detector beam (blue) is similarly mounted, whereas the detector chamber is placed on an antivibration table, isolating the beam from the environment, and minimizing the transmission of non-gravitational forces. Both chambers can be evacuated to minimize acoustical coupling effects. The detector movement is measured using three laser vibrometers (D1–D3), positioned on a separate stage, similarly isolated via springs. The red dashed lines illustrate the laser beams. By moving the transmitter chamber, distance d_0 between the beams can be varied, thus changing the magnitude of the gravitationally induced excitation force acting on the detector beam. The whole setup is located in an underground laboratory, providing excellent temperature stability and minimal seismic noise. The accelerometers measuring the chamber movement are not visible in the picture.

using a Taylor expansion under the assumption that $u_t' \ll d_0$ (equation (4)). Here $Q_d \approx (cm_d)^{1/2}\delta^{-1}$ denotes the quality factor of the oscillator, assuming small damping. Equation (1) indicates that dynamic gravitational interaction can be observed if suitable parameters are chosen. Note that the detector displacement is not directly dependent on its mass. Consequently, the dynamic acceleration amplitude will be larger by a factor of $2Q_d u_t'/d_0$ compared with the acceleration due to gravitational force in a static setup. The working principle (Fig. 1a, point masses) can be transformed into continuous bodies, such as vibrating bending beams (Fig. 1b). In this case, both transmitter and detector beams are resonating bending beams; hence, both oscillators must have similar resonance frequencies to achieve sufficient amplitudes. For the setup and measurements described in this Article, we focus on the first bending mode. To theoretically describe the interaction between the two beams, Newton's law of gravitation is applied in terms of continuum mechanics with a gravitational force field acting on the detector beam (equations (7) and (8)). Like the point mass model, the said force field is composed of three parts: a static part, a dynamic part at the frequency of excitation and a dynamic part at higher harmonics. If we apply the resulting force distribution as excitation force to the well-known equation of motion of a free–free Euler–Bernoulli beam, we get the detector beam's resonance velocity amplitude, analogously formulated to the simple point mass model via

$$\frac{v_{db,0}}{v_{tb,0}} \approx i \frac{Gm_t Q_d}{\omega_0^2} \Gamma\left(d_0, \text{parameters}\right), \tag{2}$$

where $v_{db,0}$ and $v_{tb,0}$ describe the (complex) velocity amplitudes of the bending resonance motion of the detector and transmitter,

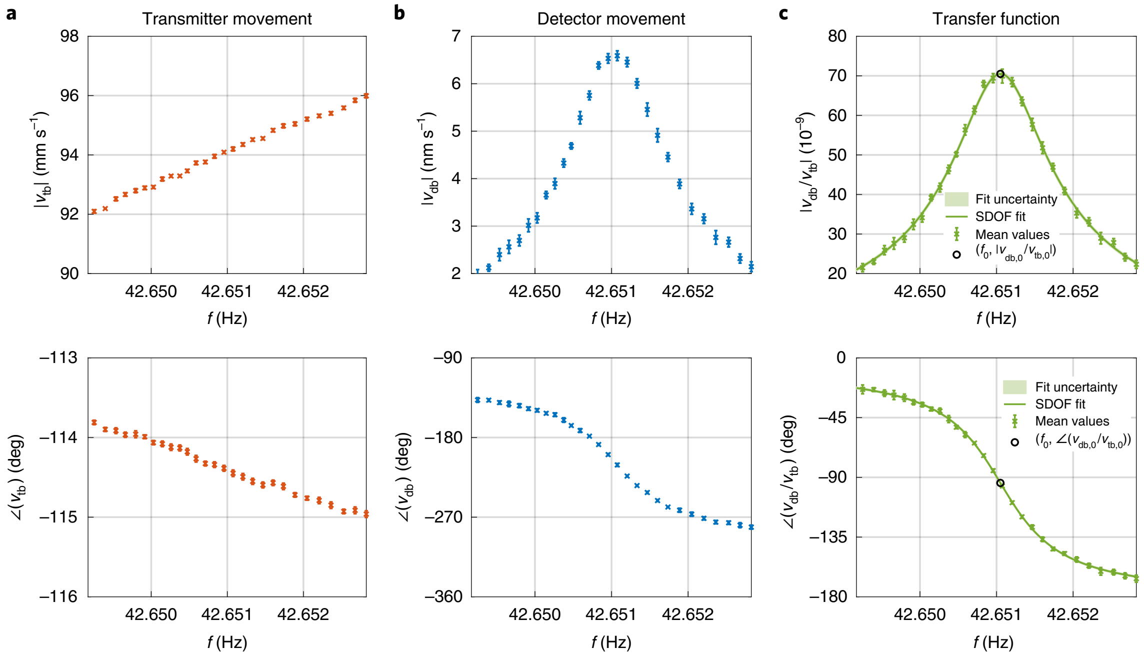

Fig. 3 | Result of a measurement run. Frequency spectra of the transmitter and detector bending velocities evaluated from subsequent excitation at 30 discrete frequencies around the first bending resonance of the detector beam at a beam distance of $d_0 = 59$ mm. (Fig. 5, 18-Mar-21-1 run). Each frequency is held for 50 min, out of which the last 25 min are averaged to obtain the mean value and standard deviation (error bars) of the amplitude/phase at each frequency. The top panels show the amplitude spectrum, denoted by absolute value brackets |…| and the bottom panels show the phase spectrum, denoted by ∠(…). **a**, Spectrum of the transmitter bending velocity v_{tb}: quasi-constant excitation with ~94 mm s^{-1} amplitude. The error bars are too small to be visible. **b**, Spectrum of the detector bending velocity v_{db}, extracted from velocity v_d measured at three positions, namely, $x_d = (0.005\,\text{m}, l_d/2 \text{ and } l_d - 0.005\,\text{m})$ (equation (14)). **c**, Transfer function spectrum calculated from v_{db} and v_{tb} and fit of an SDOF transfer function (equation (15)). The fit uncertainty illustrates the 95% confidence band. The fit allows the extraction of parameters for this measurement: resonance frequency $f_0 = \omega_0/2\pi = 42.65105015(77)$ Hz, Q factor $Q_d = 3.5827(46) \times 10^4$, amplitude ratio at resonance $|v_{db,0}/v_{tb,0}| = 70.14(13) \times 10^{-9}$ and resonance phase shift $\angle(v_{db,0}/v_{tb,0}) = -93.965(73)°$. The two latter values correspond to one data point in Fig. 4a,b. The coefficient of determination of the fit is $R^2 = 99.64\%$.

respectively. The function Γ is dependent on the distance d_0, beam's dimensions, additional moving masses and their relative positions, and can be calculated using an analytical or finite-element three-dimensional model of the setup (Methods).

Experiment design and measurement procedure

The amplitude of the detector beam is maximized by a large transmitter mass, low frequencies, small distance and high Q of the detector oscillator (equation (2)). We, therefore, selected a detector beam made of titanium of 1 m length and a rectangular cross section of 17.0 mm × 8.5 mm. The beam is hanging on two strings that are attached at the nodal points of the first bending mode to minimize both additional damping and transmission of forces from the supporting structure. An illustration of the setup is shown in Fig. 2, indicating the experimental setup and both transmitter and detector beams. The motion of the detector beam is measured using three laser interferometers (Fig. 2, D1–D3) placed on a separate, spring-suspended platform. The laser beams (Fig. 2, dashed lines) point horizontally onto the beam surface where they are reflected by small patches of retroreflective tape. The use of three measurement positions allows the extraction of the bending motion from signals that may also contain the rigid-body motion of both detector beam and laser stage (equation (14)).

The transmitter beam is made of tungsten with dimensions of 1 m × 20 mm × 10 mm and a total mass of 3,875.6(1) g. A piezoelectric transducer with a countermass at its opposite end is mounted at the centre of the beam such that the bending motion can be generated with minimal reaction forces acting on the supports. The system is designed such that the resonance frequency of the first bending mode of the transmitter is as close as possible to the first bending resonance of the detector beam (~42.65 Hz). The transmitter beam hangs on two springs that are attached at the nodal points of the first bending mode. Its displacement is measured by another laser interferometer (Fig. 2, T1).

Besides the maximization of the gravitational forces and the resulting detector motion, the prevention of any excitation or signal coupling other than gravity is of utmost importance. Therefore, both beams have been placed in separate aluminium vacuum chambers to avoid acoustic coupling effects. Further, the chamber containing the detector was placed on a vibration-isolation table, whereas the transmitter chamber is hanging on springs from a movable bar attached to a solid frame with high damping. Accelerometers mounted on both chambers give information about unwanted movement of the chambers. By means of experimental and numerical modal analysis of the whole setup, great care is taken to avoid any system resonances near the detector resonance.

Due to the high Q factor of the detector beam ($Q_d \approx 35{,}000$), the time until a steady-state vibration is reached is fairly high (time constant, $\tau \approx 260$ s). Further, long-time averaging is applied during evaluation to increase the measurement resolution. Hence, it must be ensured that the vibration conditions, especially the resonance frequency of the detector beam, remain stable during the measurement period. Therefore, the whole setup has been placed in an underground laboratory in the Swiss Alps where a very stable temperature can be guaranteed, resulting in an average temperature span of ~2×10^{-3} °C per measurement point (25 min) and 0.013 °C per total measurement (24 h). Additionally, the location shows

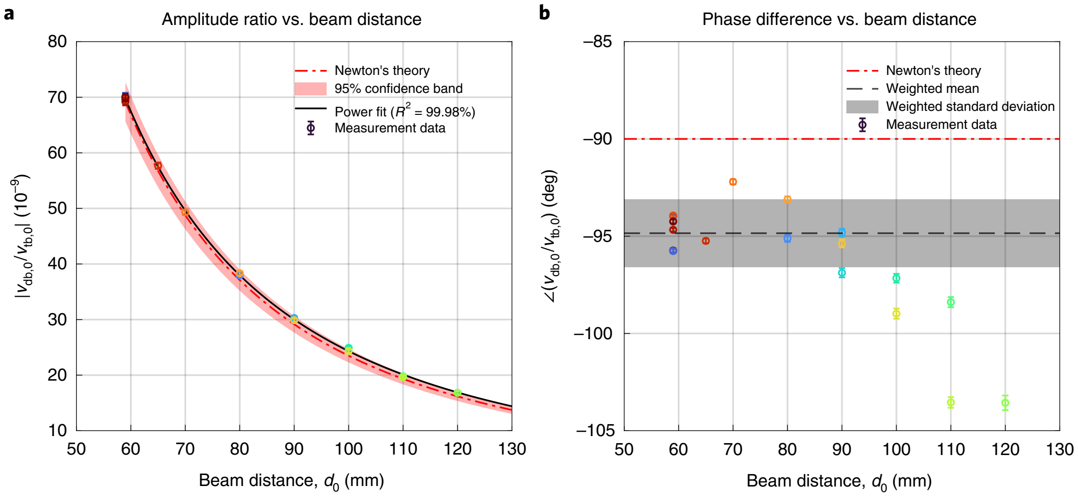

Fig. 4 | Gravitationally induced bending motion. Compilation of the SDOF fit results (equation (15)) and the associated 95% confidence interval (error bars) from all the frequency spectrum measurements at different beam distances d_0 (example shown in Fig. 3). **a**, Amplitude ratio between the detector bending velocity $v_{db,0}$ and transmitter bending velocity $v_{tb,0}$ at resonance as a function of beam distance d_0. A power-law behaviour with exponent –1.99(1) and $R^2 = 99.98\%$ (black line) can be identified. The values lie well within the confidence band (red-shaded area) of the theoretical prediction (red dash–dot line) that comprises statistical and systematic uncertainties (Table 1). **b**, Corresponding phase difference. The inverse-variance weighted mean phase shift of (−94.8 ± 1.7)° (black dashed line) is a bit lower than the theoretical prediction of −90° (red dash–dot line), suggesting minor error contributions. The grey band illustrates the inverse-variance weighted standard uncertainty. The colour scheme of the data points is the same as Fig. 5.

minimal external disturbances that comply with the VC-G vibration criterion[27].

Further details on the experimental setup and isolation measures are provided in Methods and Extended Data Table 1. During an experiment run, the piezoelectric transducer is sequentially excited with a 14 V_p sinusoidal signal at multiple frequencies around the detector bending resonance. Each frequency is held for 50 min, and the detector and transmitter velocities are measured by the laser vibrometers. Both transmitter and detector chambers are evacuated to a pressure of 1 mbar before every new frequency, yielding a constant pressure within 1% due to minor leakage. Thus, it is guaranteed that the dynamic properties of the detector remain unchanged throughout the measurement.

To extract the amplitude and phase only at the frequency of excitation, the outputs of the laser interferometers are fed into individual lock-in amplifiers, thus achieving a velocity amplitude resolution of 0.16 nm s^{-1}. The data from the last 25 min of every frequency step is averaged and used for the data evaluation, further improving the resolution.

Figure 3 shows the result of an example measurement run (30 frequencies; frequency resolution, $\Delta f = 0.126$ mHz; total duration, ~31 h). Due to the relatively high damping of the transmitter beam ($Q_t \approx 680$), the frequency spectrum of the transmitter beam reveals a nearly constant bending vibration of $v_{tb} \approx 94$ mm s^{-1} amplitude (Fig. 3a). Figure 3b shows the frequency spectrum of the detector bending velocity v_{db} around the bending resonance, derived from the velocities $v_d(x_{d,n})$ at three measurement positions $x_{d,n}$ along the detector beam (equation (14)).

The spectrum shows a clear resonance at 42.651 Hz corresponding to the considered bending mode. By taking the ratio between the response and excitation velocities, the transfer function v_{db}/v_{tb} can be derived (Fig. 3c). According to equation (2), the amplitude ratio at resonance $v_{db,0}/v_{tb,0}$ gives a measure of the gravitationally induced excitation. Note that the phase at resonance is close to −90° and not +90° as equation (2) would indicate, since the transmitter and detector lasers measure the velocity in opposite directions. Since the bending resonance can be approximated as a single-degree-of freedom (SDOF) oscillator, provided that no other resonances are close by, the well-known equation of such a system can be fitted to the measured transfer function. As a result, estimates for the detector resonance frequency, amplitude ratio at

Table 1 | One-sigma error budget used for the assessment of the combined measurement uncertainty of *G* estimated from one single measurement and from all the 18 measurements

	Relative standard uncertainty (%)	$\Delta G/G$ (%)
Systematic errors		
Detector laser vibrometer	0.67%	0.49%
Detector laser angular misalignment	0.01%	0.01%
Detector laser lock-in amplifier	0.01%	0.00%
Transmitter laser vibrometer	0.67%	0.67%
Transmitter laser angular misalignment	0.01%	0.01%
Transmitter laser lock-in amplifier	0.01%	0.01%
Transmitter beam mass, m_t	0.00%	0.00%
Beam distance, d_0	0.66%*	1.31%
Model parameter, γ	0.16%	0.16%
Statistical errors		
Fit error resonance amplitude ratio, $\lvert v_{db,0}/v_{tb,0}\rvert$	0.32%*	0.32%
Detector beam resonance frequency, ω_0	< 0.0001%*	< 0.0001%
Detector beam Q factor, Q_d	2.36%	2.36%
Beam distance, d_0	0.0001%	0.0002%
Statistical error of all measurements		0.56%
Combined error	**Single measurement**	**2.85%**
	All measurements	**1.66%**

*Arithmetic mean of all the measurements.

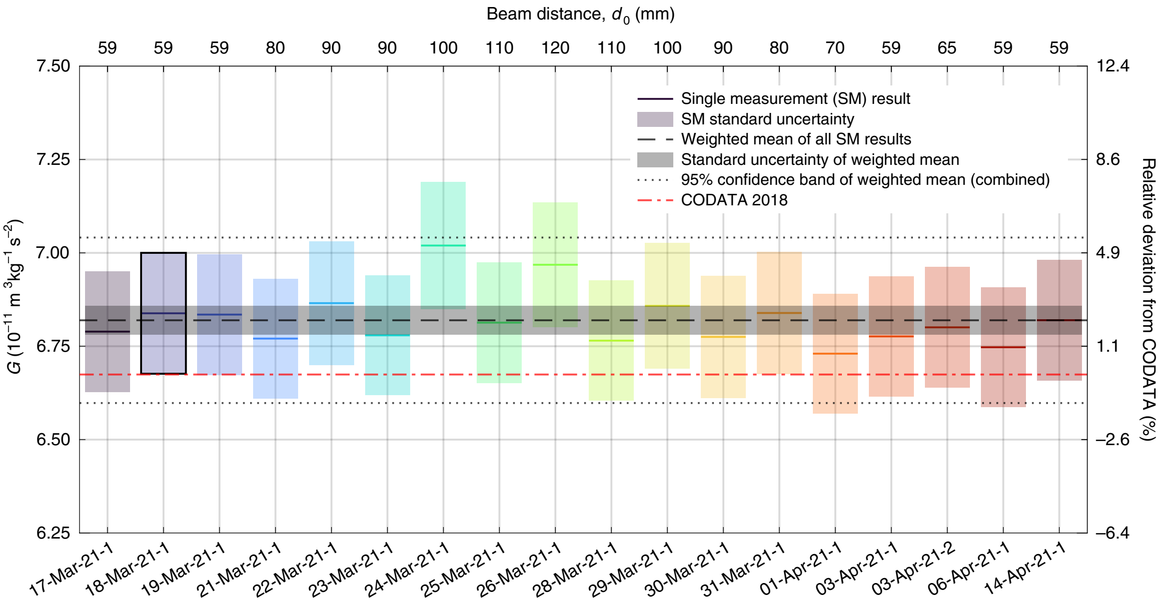

Fig. 5 | Measurement result of the gravitational constant. Over a period of four weeks, 18 single measurement runs (similar to the example shown in Fig. 3) were conducted at different beam distances d_0. Each measurement yields the amplitude ratio and phase difference between the detector and transmitter motion at resonance, which has been used to estimate the gravitational constant using equation (2). The figure illustrates the single and averaged results for G (left y axis) and the deviation from the CODATA 2018 value (right y axis). Lower x axis, measurement date; upper x axis, beam distance d_0. The result of the measurement shown in Fig. 3 corresponds to the black framed box. The calculation of G uses a fixed detector-beam Q factor of $3.595(85)\times10^4$, obtained as the weighted mean value from all the single-measurement results. Each measurement yields an estimate for G (coloured lines), together with a standard uncertainty (coloured boxes). An inverse-variance weighted mean (black dashed line) with standard uncertainty illustrated by the black-shaded area (0.56%) yields an overall estimate of $G^*=6.820\times10^{-11}\,\mathrm{m^3\,kg^{-1}\,s^{-2}}$, with a combined standard uncertainty of about 1.66%. The estimation is about 2.2% higher than the CODATA 2018 value (red dash-dot line). The plotted 95% confidence band (black dotted lines) represents the extended combined measurement uncertainty ($k=1.96$) based on statistical and systematic uncertainties (Table 1). The colour scheme of the data points is the same as Fig. 4.

resonance, Q factor and resonance phase shift are obtained (equation (15)). Here Q_d was also alternatively confirmed by a piezoelectric excitation of the system.

Examination of gravitationally induced detector vibration

Over a period of four weeks, 18 measurement runs following the measurement procedure presented in Fig. 3 were conducted at different beam distances.

The results of the complex velocity ratio at resonance $v_{\mathrm{db},0}/v_{\mathrm{tb},0}$ are summarized in Fig. 4. Each data point corresponds to a 22-point frequency spectrum, where the resonance amplitude and phase have been extracted by fitting the transfer function of an SDOF oscillator (equation (15)). The amplitude curve shows a clear power-law behaviour with exponent −1.99(1) and $R^2=99.98\%$. The excellent agreement with Newton's theory indicates that the detector motion is indeed caused by gravitational coupling and not by other effects such as mechanical or acoustical coupling.

The values lie well within the tolerance band of the theoretical prediction that comprises statistical and systematic uncertainties (Table 1). The inverse-variance weighted mean phase shift of $(-94.8\pm1.7)^\circ$ is slightly lower than the theoretical value of -90°, suggesting a minor error contribution. The deviation of the resonance phase from the theory increases with distance, whereas the standard error remains unchanged. This may indicate a systematic error due to remaining crosstalk, which becomes more prominent with a decreasing gravitational signal.

Since the temperature and pressure barely change, the Q factor of the detector beam was estimated by an inverse-variance weighted mean of all the measurement results, resulting in $Q_d=3.595(85)\times10^4$. The resonance frequency of the detector was determined to be $f_0=\omega_0/2\pi=42.650759(15)$ Hz at 11.4 °C, being linearly dependent on the temperature with coefficient $\alpha=-0.01834(56)\,\mathrm{Hz\,^\circ C^{-1}}$ (Extended Data Fig. 1).

Finally, G was estimated from each measurement result using equation (2) and the theoretical model. In Fig. 5, the single results are depicted as the mean value and standard deviation from statistical errors (coloured patches).

Combining the single measurements of G by means of inverse-variance weighting yields $G^*=6.820\times10^{-11}\,\mathrm{m^3\,kg^{-1}\,s^{-2}}$ with a relative standard deviation of about 0.56% (Fig. 5, black dashed line and grey band). The overall 95% confidence band (Fig. 5, black dotted line) represents the extended combined measurement uncertainty ($k=1.96$) based on statistical and systematic uncertainties (Table 1). Finally, G is estimated with $G^*=6.82(11)\times10^{-11}\,\mathrm{m^3\,kg^{-1}\,s^{-2}}$, which is only about 2.2% higher than the CODATA 2018 value[8].

Due to the observed deviation from the theoretical prediction (Fig. 4), that is, the deviation from the CODATA value (Fig. 5), a slight systematic error might be present, which is suspected to be a non-gravitational, mechanical coupling. During these experiments, we measured a small movement of the detector chamber with amplitudes typically about $0.25\,\mathrm{nm\,s^{-1}}$ at the frequency of excitation, which might be responsible.

Based on a power balance analysis, the near-field gravitational energy flow between the transmitter and detector can be computed. At the steady state, the incoming energy at the detector is dissipated according to the Q factor of the detector. If all this energy is attributed to gravitation, this yields a gravitational power of 2.64×10^{-20} W for the measurement run depicted in Fig. 3 (equation (13)).

Discussion and outlook

We described the gravitationally induced excitation of a bending beam resonator at around 42 Hz, which can be used to investigate the dynamic properties of gravitation and to quantify the gravitational constant. Dynamical gravitation experiment in this frequency range is particularly interesting given the recent results of gravitational waves obtained by the LIGO system[12] with frequencies in the 100 Hz regime.

However, despite amplification due to resonance, the measured amplitudes remain fairly small; hence, the measurement is extremely sensitive to external disturbances and crosstalk. The use of a higher-Q material, such as quartz glass, can improve the signal-to-noise ratio with the drawback of even longer measurement times. Crosstalk can be further reduced by an improved passive decoupling or active vibration isolation. At this early stage, the measurement uncertainty is relatively high. To provide reliable data for dynamic gravitation, the uncertainty must be considerably reduced. This requires, amongst others, a more precise beam distance control and a minimization of the temperature influence, which affect the detector's dynamic properties. Further, future work must focus on a traceable calibration of the measurement chain in the measurement range of several nanometres per second.

Motivated by another work[20], future work could also contain a non-resonant transmitter such as one or several rotating bars. This makes the excitation more flexible, which can increase the gravitational forces. Further, it enables the use of higher harmonics of the dynamic gravitational forces.

We think that this work shows the great potential of fully characterized dynamical gravitational experiments. The approach can be transferred to other continuum vibrational systems at the micro- and macroscale, thus opening a completely new field of gravitational interaction experiments and leading to newer insights in this field.

Besides a more accurate determination of G, our next goals include topics such as the investigation of the frequency dependency of G, inverse square law or gravitational shielding.

Online content

Any methods, additional references, Nature Research reporting summaries, source data, extended data, supplementary information, acknowledgements, peer review information; details of author contributions and competing interests; and statements of data and code availability are available at https://doi.org/10.1038/s41567-022-01642-8.

Received: 4 September 2021; Accepted: 19 May 2022;
Published online: 11 July 2022

References

1. Newton, I., Cohen, I. B. & Whitman, A. *The Principia: Mathematical Principles of Natural Philosophy* (Univ. of California Press, 1999).
2. Einstein, A. Die grundlage der allgemeinen relativitätstheorie. *Ann. Phys.* **354**, 769–822 (1916).
3. Speake, C. & Quinn, T. The search for Newton's constant. *Phys. Today* **67**, 27–33 (2014).
4. Gundlach, J. H. & Merkowitz, S. M. Measurement of Newton's constant using a torsion balance with angular acceleration feedback. *Phys. Rev. Lett.* **85**, 2869–2872 (2000).
5. Quinn, T., Parks, H., Speake, C. & Davis, R. Improved determination of G using two methods. *Phys. Rev. Lett.* **111**, 101102 (2013).
6. Li, Q. et al. Measurements of the gravitational constant using two independent methods. *Nature* **560**, 582–588 (2018).
7. Cavendish, H. XXI. Experiments to determine the density of the Earth. *Philos. Trans. R. Soc.* **88**, 469–526 (1798).
8. Tiesinga, E., Mohr, P. J., Newell, D. B. & Taylor, B. N. CODATA recommended values of the fundamental physical constants: 2018. *Rev. Mod. Phys.* **93**, 025010 (2021).
9. Adelberger, E. New tests of Einstein's equivalence principle and Newton's inverse-square law. *Class. Quantum Gravity* **18**, 2397–2405 (2001).
10. Hoyle, C. D. et al. Submillimeter test of the gravitational inverse-square law: a search for 'large' extra dimensions. *Phys. Rev. Lett.* **86**, 1418–1421 (2001).
11. Chiaverini, J., Smullin, S. J., Geraci, A. A., Weld, D. M. & Kapitulnik, A. New experimental constraints on non-Newtonian forces below 100 microns. *Phys. Rev. Lett.* **90**, 151101 (2002).
12. Abbott, B. P. et al. Observation of gravitational waves from a binary black hole merger. *Phys. Rev. Lett.* **116**, 061102 (2016).
13. Barish, B. C. Nobel lecture: LIGO and gravitational waves II. *Rev. Mod. Phys.* **90**, 040502 (2018).
14. Chen, Y. T. & Cook, A. *Gravitational Experiments in the Laboratory* (Cambridge Univ. Press, 1993).
15. Westphal, T., Hepach, H., Pfaff, J. & Aspelmeyer, M. Measurement of gravitational coupling between millimetre-sized masses. *Nature* **591**, 225–228 (2021).
16. Kapner, D. J. et al. Tests of the gravitational inverse-square law below the dark-energy length scale. *Phys. Rev. Lett.* **98**, 021101 (2007).
17. Quinn, T. Don't stop the quest to measure Big *G*. *Nature* **505**, 455–455 (2014).
18. Pontikis, C. Détermination de la constant de gravitation par la méthode de résonance. *C. R. Hebd. Seances Acad. Sci. Ser. B* **274**, 437–440 (1972).
19. Zahradnicek, J. Resonanz methode für die messung der gravitationsk constante mittels der drehwaage. *Phys. Zeitschr.* **34**, 126–133 (1933).
20. Sinsky, J. A. Generation and detection of dynamic Newtonian gravitational fields at 1660 cps. *Phys. Rev.* **167**, 1145–1151 (1968).
21. Hirakawa, H., Tsubono, K. & Oide, K. Dynamical test of the law of gravitation. *Nature* **283**, 184–185 (1980).
22. Astone, P. et al. Experimental study of the dynamic Newtonian field with a cryogenic gravitational wave antenna. *Eur. Phys. J. C* **5**, 651–664 (1998).
23. Long, J. C. et al. Upper limits to submillimetre-range forces from extra space-time dimensions. *Nature* **421**, 922–925 (2003).
24. Liu, Y. et al. Gravitational forces between nonclassical mechanical oscillators. *Phys. Rev. Appl.* **15**, 034004 (2021).
25. Schmöle, J. et al. A micromechanical proof-of-principle experiment for measuring the gravitational force of milligram masses. *Class. Quantum Grav.* **33**, 125031 (2016).
26. Walker, W. D. *Gravitational Interaction Studies*. PhD thesis, ETH Zürich (1997).
27. Gordon, C. G. Generic vibration criteria for vibration-sensitive equipment. *Proc. SPIE Optomech. Eng. Vib. Control* **3786**, 22–33 (1999).

Methods

Theory. *Point mass model.* The equation of motion of the detector mass (Fig. 1a) is given by

$$m_{\mathrm{d}}\ddot{u}_{\mathrm{d}}+\delta\dot{u}_{\mathrm{d}}+cu_{\mathrm{d}}=-F_G=-G\frac{m_{\mathrm{d}}m_{\mathrm{t}}}{d^2},\qquad(3)$$

where δ is the damping constant; c, the spring constant; u_{d}, the detector mass displacement with respect to its reference position; d, the distance of the masses m; and F_G, the gravitational force according to Newton's law of gravitation[1,28]. Indices 't' and 'd' indicate the element being a part of the transmitter or detector, respectively. A superposed dot denotes the time derivative. We assume low damping $\delta \ll 2(cm_{\mathrm{d}})^{1/2}$. The transmitter mass is oscillating with amplitude u_{t}' and angular excitation frequency ω; hence, the distance between the masses changes periodically with $d=d_0-u_{\mathrm{t}}'\mathrm{e}^{\mathrm{i}\omega t}$. Assuming $\varepsilon=u_{\mathrm{t}}'/d_0\ll 1$ allows us to approximate the force with a Taylor expansion around $\varepsilon=0$ as

$$F_G\approx\frac{Gm_{\mathrm{d}}m_{\mathrm{t}}}{d_0^2}+\frac{2Gm_{\mathrm{d}}m_{\mathrm{t}}}{d_0^3}u_{\mathrm{t}}'\mathrm{e}^{\mathrm{i}\omega t}+O\left(\varepsilon^2\right)\qquad(4)$$

representing a static component, a dynamic part at frequency ω and negligible terms of higher order in ε. Instead of using the Taylor approximation, full nonlinearity can be considered by computing the Fourier series coefficient c_1 at frequency ω, that is,

$$F_{G,\omega}=c_1\mathrm{e}^{\mathrm{i}\omega t};\,c_1=\frac{2\pi}{\omega}\int_0^{\frac{2\pi}{\omega}}F_G\left(t\right)\mathrm{e}^{-\mathrm{i}\omega t}\mathrm{d}t.\qquad(5)$$

Introducing the angular resonance frequency $\omega_0=(c/m_{\mathrm{d}})^{1/2}$ and quality factor $Q_{\mathrm{d}}\approx(cm_{\mathrm{d}})^{1/2}\delta^{-1}$, the detector mass displacement is given by the well-known solution of equation (3) as[29]

$$u_{\mathrm{d}}=-\frac{F_G}{m_{\mathrm{d}}}\frac{1}{\omega_0^2-\omega^2+\frac{\mathrm{i}\omega\omega_0}{Q_{\mathrm{d}}}}.\qquad(6)$$

When exciting at resonance ($\omega=\omega_0$), the maximum displacement amplitude of the detector is obtained (equation (1)). Because Q_{d} is of the order of 10^4 and higher, the static component and higher-order terms can be neglected in the vicinity of ω_0.

Beam model. Assuming continuous bodies (Fig. 1b), the gravitational interaction can be formulated in terms of continuum mechanics, which yields the gravitational force in the y direction between two infinitesimal mass elements dm of the detector and transmitter beams given by

$$F_{Gy}^{(\mathrm{d}m_{\mathrm{d}}-\mathrm{d}m_{\mathrm{t}})}=-G\frac{\mathbf{r}\cdot\mathbf{e}_y}{\|\mathbf{r}^3\|}\mathrm{d}m_{\mathrm{d}}\mathrm{d}m_{\mathrm{t}};\mathbf{r}=\mathbf{r}_{\mathrm{d}m_{\mathrm{d}}}-\mathbf{r}_{\mathrm{d}m_{\mathrm{t}}}\qquad(7)$$

where position vectors $\mathbf{r}_{\mathrm{d}m}$ are of the mass elements dm and unit vector $\mathbf{e}_y$ is in the y direction. The position vectors include amplitude (u_{tb}' and u_{db}', respectively), frequency ω and shape of the beam's centre-line displacements that can be derived from the well-known Euler–Bernoulli beam theory using free–free boundary conditions[30]. The use of this linear theory for the first bending mode is justified because the beams are slender (thickness/wavelength, $h/\lambda\approx 0.01$; width/wavelength, $w/\lambda\approx 0.01$) and the displacement amplitudes u are small ($u\ll h, w$). The x displacements (Fig. 1b) are neglected as they are of the order of $(h/\lambda)\times \mathrm{d}u/\mathrm{d}x_{\mathrm{t}}$. Note that the mode shapes of the detector and transmitter slightly differ due to the additional mass of the piezo-transducer and countermass mounted on the transmitter beam. Consequently, the gravitational force distributed along the central axis of the detector beam can be derived by integrating over the transmitter beam volume V_{t} and detector beam cross-sectional area A_{d}, which yields the force per unit length in the y direction:

$$\begin{aligned}F_{Gy}\left(x_{\mathrm{d}},t\right)&=-G\rho_{\mathrm{d}}\rho_{\mathrm{t}}\int_{(V_{\mathrm{t}})}\int_{(A_{\mathrm{d}})}\frac{\mathbf{r}\cdot\mathbf{e}_y}{\|\mathbf{r}^3\|}\mathrm{d}V_{\mathrm{t}}\mathrm{d}A_{\mathrm{d}}\\&\approx-G\rho_{\mathrm{d}}\rho_{\mathrm{t}}\left(f_{Gy,0}\left(x_{\mathrm{d}}\right)+f_{Gy,1}\left(x_{\mathrm{d}}\right)\mathrm{e}^{\mathrm{i}\omega t}\right)\end{aligned}\qquad(8)$$

as a function of detector coordinate x_{d}, where ρ denotes the material density, assuming a homogeneous mass distribution in each beam. Similar to the point mass model, a Taylor series approximation around $\varepsilon=u_{\mathrm{t}}'/d_0=0$ can be applied, yielding a static part f_{Gy0}, a dynamic part $f_{Gy1}\,\mathrm{e}^{\mathrm{i}\omega t}$ containing the frequency of excitation, and higher-order terms $O(\varepsilon^2)$. Alternatively, a Fourier series can be used if the nonlinearity of the gravitational force must be taken into account (equation (5)). For the small vibration amplitudes used in the experiment, however, the two approaches yield very similar results with a difference of less than 0.5%. For F_{Gy}, we neglect the influence of the very small, gravitationally induced detector motion as it has a negligible influence ($u_{\mathrm{d}}'<10^{-7}u_{\mathrm{t}}'$). The solution of detector motion can be found using the eigenfunction expansion method[30], where a particular solution of the form

$$u_{\mathrm{d}}\left(x_{\mathrm{d}},t\right)=u_{\mathrm{dT}}\left(t\right)U_{\mathrm{dT}}\left(x_{\mathrm{d}}\right)+u_{\mathrm{dR}}\left(t\right)U_{\mathrm{dR}}\left(x_{\mathrm{d}}\right)+\sum_{n=1}^{\infty}u_{\mathrm{db},n}\left(t\right)U_{\mathrm{db},n}\left(x_{\mathrm{d}}\right)\qquad(9)$$

is considered. Here U_{dT} and U_{dR} denote translational and rotational rigid-body movements with corresponding contribution factors u_{dT} and u_{dR}, respectively, whereas $U_{\mathrm{db},n}$ are the normalized eigenfunctions ($U_{\mathrm{db},n}(0)=1$) and $u_{\mathrm{db},n}$ are the corresponding modal coordinates[30]. When the excitation frequency is close to a particular resonance frequency (in our case, the resonance frequency of the first bending mode, $\omega_0=\omega_{\mathrm{b},1}$), it can be shown—based on the orthonormality relation of the eigenfunctions and symmetry properties of the force field—that the contributions of all the other modes are negligible. This applies for rigid-body movements, too. The amplitude of the corresponding modal coordinate is, thus, found by the solution of the first-order ordinary differential equation as

$$\ddot{u}_{\mathrm{db},1}+\frac{\omega_0}{Q_{\mathrm{d}}}\dot{u}_{\mathrm{db},1}+\omega_0^2u_{\mathrm{db},1}=-\frac{4G\rho_{\mathrm{d}}\rho_{\mathrm{t}}}{m_{\mathrm{d}}}\int_0^{l_{\mathrm{d}}}U_{\mathrm{db},1}\left(x_{\mathrm{d}}\right)f_{Gy,1}\left(x_{\mathrm{d}}\right)\mathrm{e}^{\mathrm{i}\omega t}\mathrm{d}x_{\mathrm{d}},\qquad(10)$$

where modal damping is specified with quality factor Q_{d} of the detector beam. When the steady state is reached, the detector motion is obtained from the particular solution of equation (10), that is,

$$u_{\mathrm{db}}\left(x_{\mathrm{d}},t\right)=u_{\mathrm{db}}'\,U_{\mathrm{db},1}\left(x_{\mathrm{d}}\right)\mathrm{e}^{\mathrm{i}\omega t},\qquad(11)$$

where u_{db}' is the gravitationally induced bending vibration amplitude at measurement position x_{d}. The integral in equation (10) can be simplified by a transformation to dimensionless variables (denoted with the bar accent in equation (12)). Then, the detector displacement amplitude is obtained using equation (2), which contains the frequency dependence given in equation (6), the easy-to-measure properties of the experiment and a sixth-order integral over all the spatial coordinates. The integral can be computed with arbitrary precision using a numeric computing environment (we used Maplesoft Maple 2020).

$$u_{\mathrm{db}}{\prime}=u_{\mathrm{t}}'\frac{-Gm_{\mathrm{t}}}{\omega_0^2-\omega^2+\frac{\mathrm{i}\omega\omega_0}{Q_{\mathrm{d}}}}\underbrace{4\int_{\bar{V}_{\mathrm{t}}}\int_{\bar{V}_{\mathrm{d}}}\bar{U}_{\mathrm{db},1}\bar{f}_{Gy,1}\left(\bar{x}_{\mathrm{d}}\right)\mathrm{d}\bar{V}_{\mathrm{d}}\mathrm{d}\bar{V}_{\mathrm{t}}}_{\Gamma\left(d_0,\ \text{beam coordinates, beam dimensions}\right)}\qquad(12)$$

The gravitational influence of other moving masses such as the transducer and countermass are similarly calculated, resulting in an additional excitation force. Note that due to the varying distance of individual points on the beams, Γ is not proportional to d_0^{-3} as in the case of point masses. However, for the setup and parameters presented here, the integral term including all the exciting masses can be well approximated by $\Gamma\approx d_0^{-2}$, where Γ has units of m^{-3}.

Limitations and prospects of the model. Here some limitations of the theoretical model are briefly discussed.

Regarding the approximation methods, the Taylor approximation is favourable, since only a sixth-order integral must be solved. However, if $u_{\mathrm{t}}'/d_0\ll 0$ does not hold anymore, a Fourier approximation will be the better choice. Generally, a Fourier approximation is preferred if computational power is not limited, since it considers the full nonlinearity of the gravitational force field. For small distances, the excitation force might contain non-negligible amplitudes at higher harmonics of the excitation frequency that might excite other vibration modes of the detector beam. Although the lock-in measurement technique enables the extraction of motion at one specific mode/frequency, the said harmonics might add a certain error to the results. A multimodal analysis, that is, additional measurements at higher harmonics, could be used to even better quantify the gravitational coupling.

Energy considerations. When the steady state is reached, the energy stored in the vibration of the detector beam can be calculated from the kinetic energy at the maximum beam velocity, that is,

$$E_{\mathrm{stored}}=\frac{1}{2}\rho_{\mathrm{d}}A_{\mathrm{d}}\omega^2u_{\mathrm{db}}'^2\int_0^{l_{\mathrm{d}}}U_{\mathrm{db},1}\left(x_{\mathrm{d}}\right)^2\mathrm{d}x_{\mathrm{d}}.\qquad(13)$$

For a bending amplitude of $u_{\mathrm{db}}'=24.6$ pm (resonance amplitude of the 18-Mar-21-1 run; Fig. 3b), the stored energy is 3.54×10^{-18} J. According to the definition of Q factor as 2π times the ratio between the stored energy and energy dissipated per cycle[31], the dissipated energy can be calculated using the measured Q factor of the detector beam ($Q_{\mathrm{d}}=3.595\times10^4$). If we assume that the only source that introduces energy into the detector beam is the gravitational force, the time-averaged energy flow from the transmitter to detector beam must be equal to the energy dissipated in the detector beam to maintain the vibration. For our experiments, we obtain a gravitational energy flow of $2.64\times10^{-20}\,\mathrm{J\,s^{-1}}$ during resonance excitation in the 18-Mar-21-1 run. Consequently, the gravitational energy flow decreases according to d_0^{-4} since the detector bending amplitude depends on approximately d_0^{-2}.

Experimental setup. Because of the weak nature of gravitational interaction, great care must be taken to minimize undesired effects. In particular, one has to make sure that no other vibrational modes exist in the vicinity of the excitation frequency. Because of the high Q factor (>10^4) of the used detector mode, the desired motion is then strongly amplified in comparison to all the other contributions. To maximize the amplitudes, a low frequency, small distance d_0 and large transmitter mass m_t are desired. At the same time, dimensions compatible with an easily accessible laboratory setup and vacuum chambers must be used to make a thorough and contactless investigation of non-gravitational crosstalk effects possible. The setup is fully remote controlled and automated using LabVIEW to avoid disturbances by the operators.

Transmitter beam. The transmitter beam has a length of 1.00038(1) m with a rectangular cross section of 20.07(1) mm × 10.05(1) mm. To have different resonance frequencies for the bending modes in the z and y directions, the area moment of inertia must be different for the two directions. For precise machinability, a rectangular cross section was chosen. The mass of the transmitter is 3,875.6(1) g, the Q factor of the first bending mode (internal + external damping) is ~680 at low amplitudes. The transmitter resonance was measured to be 42.58 Hz. Due to the relatively small Q factor and small transmitter nonlinearity, sufficient vibration amplitude is achieved in the vicinity of the detector resonance frequency of 42.651 Hz, making transfer function measurements possible. The beam has been cut from 99.95% pure tungsten sheet material (ASTM B760). It is hanging on taut stainless steel springs of 44 mm length (spring constant, ~0.94 N mm^{-1}) attached to the nodal points of the first bending mode to minimize the transmission of forces to the transmitter chamber. Due to the inertial excitation by piezoelectric elements, no external forces are applied. The nodal points are calculated using the Euler–Bernoulli beam theory, including an attached mass at the centre of the beam of 690 g. Small nonlinearities due to the relatively high amplitude of the transmitter can be seen in the transmitter's frequency response. However, the displacement function is assumed to be negligibly influenced as the ratio $u_t'/l_t < 10^{-3}$.

Detector beam. The detector beam is made from grade 2 titanium (3.7035) and has a length of 1.00000(1) m with a rectangular cross section of 16.97(1) mm × 8.49(1) mm. The mass of the detector beam is 647.72(2) g. Titanium has been selected because of its high Q factor amongst metals[32]. The beam is isolated from the environment by hanging on ethylene propylene diene monomer (EPDM) rubber strings of 3 mm diameter and 268 mm length that can be precisely glued to the nodal points of the first bending mode. EPDM was chosen due to its low mechanical impedance, which makes it favourable to minimize mechanical coupling. To further improve the decoupling, a mass of 7.1 g has been placed in the centre of each rubber wire. Since the EPDM strings showed a certain creep behaviour, they have been loaded for several weeks with a mass similar to the detector beam until the length was stable. During the experiments, an elongation of the wires of less than 0.5 mm per week was monitored, resulting in an increase in beam distance d_0 of <0.0035% at $d_0 = 59$ mm. Due to its creep behaviour, EPDM was considered to be unsuitable for the suspension of the heavier transmitter beam.

Excitation. For the excitation of the transmitter beam, a preloaded piezoelectric transducer (PI P-843.60) is mounted at the centre of the beam. To increase the effectivity of excitation, a countermass of 592 g is mounted at the opposite end of the actuator, yielding a dynamic force of 0.566(3) N$_p$ at an excitation amplitude of 14 V$_p$ at 42.651 Hz (PI E-505 amplifier).

The excitation signal is provided by an SRS FS740 time and frequency system, which acts as a time base for the whole experiment. The device has a phase noise of <−130 dBc Hz^{-1} and frequency stability of <10^{-12} (Allan deviation[33]).

Distance. The distance between the beams was adjusted by moving the transmitter chamber that is hanging on 12 springs from two stiff bars mounted on two parallel, synchronized linear motors (Bosch Rexroth CKK-200-NN-1 with IndraDrive HCS01 control), which can move with micrometre precision. However, the initial distance d_0 could not be precisely maintained yet, resulting in a systematic distance uncertainty of 0.5 mm.

Laboratory location/seismic noise. To obtain the highest temperature stability together with minimal seismic noise, the measurement equipment was installed in a former underground military facility in the Swiss Alps. Before the installation, the room was characterized in terms of its vibration characteristics by an external company, using a Syscom MR3000TR/MS2003+ triaxial geophone. The measurement revealed excellent conditions with floor vibrations that undercut the VC-G vibration criterion[27] (<0.8 μm s^{-1}) by about a factor of 20. The passive temperature stability of the room itself is excellent with temperature variations of less than 0.04 °C h^{-1}, two days after the persons have left the rooms. The experiment is distributed across three rooms: the measurement room containing the vacuum chambers, beams, sensors and a minimum of other equipment; the control room where all the computers, controls and remote connectivity are located; and the pumping room containing the vacuum pumps and a dehumidifier.

Velocity measurement. The movement of the detector beam was measured with three separate laser interferometers (Polytec OFV-505 laser head and Polytec OFV-5000 controller with VD-06 decoder) that are placed on a separate mount (Fig. 2), connected by weak springs to a solid support. The laser beams point horizontally and orthogonally (deviation, ±1°) onto the beam surface where they are reflected by 10 mm × 10 mm patches of retroreflective tape (3M Scotchlite 7610) sticking on the beam's surface. The mass of the tape is considered negligible (0.02 g per patch). The laser vibrometers provide a velocity resolution of ~10 nm s^{-1} Hz$^{-1/2}$, which yields a measurement resolution of ~0.37 nm s^{-1} using an eighth-order 1.37 mHz low-pass lock-in amplifier with a time constant of 31.32 s (Zurich Instruments MFLI). The inputs of the lock-in amplifiers are attenuated by a factor of 4 to prevent overload damage of the 3 V input stages of the MFLI. This could happen if the lasers lost focus, which results in voltages of 10 V (an extremely rare event). To quantify the resolution and quality of the velocity measurement, calibration measurements have been conducted before the experiments. For this purpose, one of the laser heads was adjusted to point onto a small piezoelectric transducer (10 mm × 10 mm × 1 mm) glued onto a solid steel block. Apart from that, the measurement setup remained unchanged. The transducer was driven with different excitation amplitudes at 42.6 Hz, resulting in velocities up to 10 nm s^{-1}. Measurements with zero amplitude revealed a noise level in the range of 0.16 nm s^{-1} (50 points of averaging), whereas standard deviations of signals in the range of the highest amplitudes measured in this paper (~7 nm s^{-1}) showed 0.1 nm s^{-1}. These numbers are even better than the aforementioned expected resolution. Consequently, signals greater than 1.6 nm s^{-1} can be measured with a signal-to-noise ratio greater than 10. This can be further improved by longer averaging and/or larger lock-in time constants. Considering a fixed frequency of 42.6 Hz, 1.6 nm s^{-1} corresponds to a displacement resolution of 0.6 pm since $v = \omega u$. Since the amplitudes are small in these calibration measurements, the behaviour of the piezo can be assumed to be linear and an amplitude sweep was conducted to reveal nonlinear effects of the measurement chain. The amplitude range was selected to be similar to the measurement range in the experiments. A linear fit of the excitation amplitude versus velocity data points revealed a nonlinearity of <2%$_{\mathrm{FSO}}$, where the full-scale output (FSO) is 8 nm s^{-1}. Note that this measurement also contains nonlinearities in the excitation chain (for example, the driving of the piezo), which is different from the excitation in the experiments.

Vibration isolation and measurement. Acoustical isolation. To avoid the transmission of forces due to sound waves, each chamber was evacuated with a vacuum pump (Edwards nXDS 10i vacuum scroll pump) via remote-controlled valves. Pressure evacuation was done before every frequency step, whereas no data were acquired during evacuation. The pressure increase in the chambers for pressures greater than 0.5 mbar was measured to be 22 μbar h^{-1} for the detector chamber and 155 μbar h^{-1} for the transmitter chamber.

Mechanical isolation. Besides the suspension of both beams and transmitter chamber, the detector chamber was placed on an aluminium vibration-isolation table (Opta HDT 200 anti-magnetic table with DMT 1400 base).

Electrical isolation. To minimize electrical coupling of the excitation signal into the measurement chain, for example, via ground loops containing the excitation frequency, all the relevant devices have been connected in a star ground layout to the main power source. Any high-power sources were disconnected during the measurement. Further, the detector beam and vacuum chambers were electrically grounded to avoid patch charges and creating Faraday cages.

Mechanical crosstalk measurement. Despite the thorough vibration isolation, minor transmission of forces and signals were detected at the measurement frequency. We assume these effects to be responsible for the remaining uncertainties and deviations in the measurement results. During the measurements presented in this Article, we measured a movement of the transmitter chamber of 0.82(2) μm s^{-1} in the y direction and 0.15(2) μm s^{-1} in the z direction using a Brüel & Kjær 4535-B-001 triaxial accelerometer. A certain movement of the transmitter chamber, however, is not critical if it does not excite the detector beam in its bending mode. The movement of the detector chamber was measured using two Kinemetrics EPI ES-T FBA triaxial accelerometers placed on top of the chamber. These accelerometers provide a resolution of ~1.4 pm s^{-1} when combined with an eighth-order 1.37 mHz low-pass lock-in amplifier. Typically, we measured the detector-chamber velocities as ~0.25 nm s^{-1} in the y direction and ~0.40 nm s^{-1} in the z direction at the frequency of excitation.

Post-processing/data evaluation. *Offset correction.* To eliminate possible errors due to a frequency-independent offset value of the measurement chain, an additional measurement at a frequency far away from the detector resonance has been made before each measurement run (here we used 40.44 Hz). Thus, the signal level with active piezo-excitation can be determined and subtracted from the measurement output, also eliminating electrically coupled signals produced by the amplifier of the piezo-excitation. The typical offset value measured by the lock-in amplifiers was in the range of 0.3 nm s^{-1}.

Bending amplitude extraction. Due to the detector beam suspension, rigid-body movements occur as pendulum movements with resonance frequencies around 1 Hz, velocity amplitudes up to 6 μm s^{-1} and very high time constants. Once excited by additional disturbances, they might remain for a long time and are therefore still observed in the measurements. Despite their low resonance, they may have a contribution to the velocities measured at the frequency of excitation, too.

Therefore, the measurement setup uses three lasers to extract the amplitude of the first bending mode from the combined motion as

$$u_{\mathrm{d}}\left(x_{\mathrm{d}}\right) = \left(u'_{\mathrm{dT}} + u'_{\mathrm{dR}}\left(\frac{2}{l_{\mathrm{d}}}x_{\mathrm{d}} - 1\right) + u'_{\mathrm{db},1}U_{\mathrm{db},1}\left(x_{\mathrm{d}}\right)\right)\mathrm{e}^{\mathrm{i}\omega t} \qquad (14)$$

measured by the lasers. The first bending mode shape $U_{\mathrm{db},1}$ is described by the well-known normalized solution of an Euler–Bernoulli bending beam with free–free boundary conditions[30]. Using the measured displacement/velocity at the three measurement positions $x_{\mathrm{d}} = (0.005\,\mathrm{m}, l_{\mathrm{d}}/2 \text{ and } l_{\mathrm{d}} - 0.005\,\mathrm{m})$ of the detector beam, the amplitudes u_{dT}', u_{dR}' and $u_{\mathrm{db},1}'$ can be calculated by solving the system of equations that results from equation (14); hence, the pure bending motion can be extracted. Note that the index '1' denoting the first bending mode is omitted in the main text for the sake of readability. Typical rotational and translational movements of the detector at the measurement frequency were in the range of 0.1 nm s^{-1}. For the transmitter, the rigid-body movements can be considered negligible compared with the relatively large bending motion; hence, one transmitter measurement position is sufficient.

Temperature correction. From preliminary experiments, a linear temperature dependency of the detector resonance frequency was found (temperature coefficient, $\alpha = -0.01834(56)\,\mathrm{Hz}\,^{\circ}\mathrm{C}^{-1}$; Extended Data Fig. 1). Since the temperature might slightly change during a measurement, the resonance frequency changes, too, thus producing a deviation in the frequency response from the expected SDOF behaviour. Assuming that the temperature behaviour is equal for all the frequencies around resonance, we compensated for this effect by subsequently shifting the excitation frequencies with respect to the mean temperature of the measurement. Due to the very stable temperature inside the detector chamber, the average temperature span during the whole measurement period of ~24 h was 0.013 °C. Therefore, this effect had a negligible influence on the overall results.

SDOF fit. The quantification of gravitational coupling between the two beams requires the knowledge of the response amplitude of the detector and its vibrational properties. It has been shown that the frequency response of the detector beam around the resonance can be modelled by the response of an SDOF oscillator. Thus, the theoretical equation of the transfer function (TF) of an SDOF oscillator,

$$\mathrm{TF}\left(\omega\right) = \frac{A_0\,\frac{\omega_0^2}{Q_{\mathrm{d}}}}{\omega_0^2 - \omega^2 + \frac{\mathrm{i}\omega\omega_0}{Q_{\mathrm{d}}}}\,\mathrm{e}^{\mathrm{i}\phi_0} + \mathrm{XT}, \qquad (15)$$

is fitted to the measured transfer function that is obtained from the detector bending velocity and bending velocity of the transmitter beam. Here A_0 denotes the amplitude ratio at the resonance frequency ω_0, corresponding to $|u_{\mathrm{db},0}/u_{\mathrm{tb},0}|$ (Fig. 3), and Q_{d} is the Q factor of the detector's first bending mode. As additional parameters, the phase at resonance ϕ_0, corresponding to $\angle(u_{\mathrm{db},0}/u_{\mathrm{tb},0})$ (Fig. 3), is introduced to account for eventual deviations from the theoretical prediction ($\phi_0 = -\pi/2$). Further, a complex offset XT is introduced to include frequency-independent crosstalk. The fitting is carried out using MATLAB R2021a using a Levenberg–Marquardt nonlinear least squares solver. To assess the uncertainties of the individual parameters, a bootstrapping method has been applied that uses 100 individual fits based on randomly sampled data (with replacement)[34].

Uncertainty estimation. Although at a proof-of-principle state, an estimation of the measurement uncertainties of our experimental results is presented in this section. It should be noted, however, that this Article presents a fully characterized experiment in uncharted territory with the benefits of a dynamical measurement; hence, the assessment of uncertainty should be regarded as both preliminary and an attempt to stimulate further ideas around this interesting aspect.

In estimating the uncertainty associated with measuring G, equation (2) is used to assess the influence of different variables. Therefore, one needs to evaluate the contribution of function Γ to the overall error, too. This is a rather challenging task since the function depends on several parameters in a highly nonlinear fashion. Motivated by theory and experiment, a power-law model γd_0^{-2} is stipulated to be able to move forward with the assessment. This has the merit to enable us to focus on estimation of parameter γ. Thus, assuming uncorrelated input quantities, the combined standard uncertainty can be calculated from equation (2) using a first-order Taylor approximation.

Velocity measurement. The velocity amplitudes of both transmitter and detector have been measured using commercial laser vibrometers with subsequent lock-in amplifiers. We identified the main contributions to the measurement uncertainty to be the calibration error (maximum ±1.00%), linearity error (maximum ±0.10%) and frequency-response error (maximum ±0.58%) of the vibrometers, as specified in the data sheet of the used instruments and measurement range.

However, it is yet unclear if the specified uncertainties apply equally to the small measurement amplitudes of several nanometres per second, since the calibration has been performed at considerably higher amplitudes. Therefore, a traceable calibration of the measurement chain is essential for future accurate measurement. Despite numerous challenges reported in the literature[35,36], we believe that stable temperatures and narrow bandwidth will be favourable in this regard.

Further, the input-gain accuracy of the lock-in amplifiers (maximum ±0.01%) and angular alignment of the laser beam with respect to the detector/transmitter surface (maximum ±1.00°) contribute to the uncertainty. Since the detector bending amplitude is calculated from a linear combination of three laser measurement signals (equation (14)), the contribution to the combined uncertainty must be calculated accordingly.

System parameters. The transmitter mass m_{t} has been measured with a Mettler Toledo XP6002S scale with reported linearity error of ±0.0005%, reproducibility of ±0.00013% and sensitivity deviation of ±0.0015%, resulting in an absolute standard uncertainty of the transmitter mass of better than 100 mg. The distance d_0 was initially adjusted manually, where a systematic error of ±0.5 mm was assumed. The automatic positioning system itself works very precisely with an error of ±1 µm.

Since d_0 is different for single measurements, an average relative standard error was calculated.

The Q factor of the detector is assumed to be constant since pressure and temperature are held constant throughout the measurements. Hence, its value is obtained from an inverse-variance weighted mean of all the SDOF fit results, resulting in $Q_{\mathrm{d}} = 3.595(85) \times 10^4$. The uncertainty of the resonance frequency is determined from a linear fit of the resonance frequency versus temperature curve (Extended Data Fig. 1).

SDOF fit. The error of the measured amplitude ratio and phase shift is individually obtained from each SDOF fit. To assess the contribution to the overall combined standard uncertainty of the measured G, average values were calculated.

Theoretical model. To evaluate the relative error for estimating γ, computations of the partial derivatives of γ with respect to the beam dimensions have been performed to come up with a reasonable value. Errors due to linearization of the model or other numerical effects were not considered at this phase of the project. The standard uncertainty of γ was estimated to be 0.16% using a measurement uncertainty of 0.01 mm for all the dimensions included in the model.

All uncertainty contributions are summarized in the error budget presented in Table 1. The Q factor of the detector beam, distance d_0 and velocity measurement represent the biggest error sources for the measurements presented in this paper.

Outlook. Due to the relatively large contributions of single variables, the assessment of uncertainty should be regarded as preliminary and yet incomplete. Therefore, measures to improve the uncertainty as well as unconsidered contributions are briefly discussed: using a more sophisticated beam alignment, for example, using optical methods, the initial distance accuracy may be substantially reduced. Further, a calibration of the velocity measurement chain must be performed. According to the manufacturer, the calibration uncertainty of the laser vibrometer results almost totally from the available velocity standards. However, since we are only interested in the ratio between the measured velocity signals, a relative calibration of the measurement chains increases the measurement accuracy, nonetheless.

Influences that are considered negligible at the moment might play a role if the major uncertainty contributions decrease. This can, amongst others, comprise the following.

- Beam parallelism
- mass distribution of the beams
- movement of the transmitter chamber
- nonlinear theory of the transmitter beam displacement
- influence of the Taylor approximation
- model of the piezoelectric excitation

Data availability

Source data are provided with this paper. The data that support the findings of this study are available as an open access dataset[37] or from the corresponding author upon reasonable request.

References

28. Cremer, L., Heckl, M. & Petersson, B. A. T. *Structure-Borne Sound: Structural Vibrations and Sound Radiation at Audio Frequencies* (Springer, 2005).
29. Meirovitch, L. *Fundamentals of Vibrations* (McGraw-Hill Higher Education, 2001).
30. Hagedorn, P. & DasGupta, A. *Vibrations and Waves in Continuous Mechanical Systems* (Wiley, 2007).
31. Jackson, R. G. *Novel Sensors and Sensing* (CRC Press, 2004).
32. Zhang, J., Perez, R. J. & Lavernia, E. J. Documentation of damping capacity of metallic, ceramic and metal-matrix composite materials. *J. Mater. Sci.* **28**, 2395–2404 (1993).
33. Robins, W. P. *Phase Noise in Signal Sources: Theory and Applications* (IET, 1984).

34. Efron, B. Bootstrap methods: another look at the jackknife. *Ann. Stat.* **7**, 1–26 (1979).
35. Weichert, C. et al. A heterodyne interferometer with periodic nonlinearities smaller than ±10 pm. *Meas. Sci. Technol.* **23**, 094005 (2012).
36. Pisani, M. et al. Comparison of the performance of the next generation of optical interferometers. *Metrologia* **49**, 455–467 (2012).
37. Brack, T. Dataset for the article 'Dynamic measurement of gravitational coupling between resonating beams in the Hertz regime'. ETHZ Research Collection https://doi.org/10.3929/ethz-b-000533207 (2022).

Acknowledgements

We gratefully acknowledge the support of ETH Zurich, maxon motor ag and ZC Ziegler Consultants AG. We received no specific funding for this work.

Author contributions

T.B., B.Z., F.P., J.-C.T., S.B., D.S. and J.D. designed and constructed the experiment. T.B., B.Z. and J.D. conducted the experiments, T.B., F.B. and J.D. evaluated the data and analysed the results. T.B., S.K., J.F. and J.D. derived and evaluated the theory. All the authors wrote and reviewed the manuscript.

Competing interests

The authors declare no competing interests.

Additional information

Extended data is available for this paper at https://doi.org/10.1038/s41567-022-01642-8.

Supplementary information The online version contains supplementary material available at https://doi.org/10.1038/s41567-022-01642-8.

Correspondence and requests for materials should be addressed to Jürg Dual.

Peer review information *Nature Physics* thanks Andrei Metrikine and the other, anonymous, reviewer(s) for their contribution to the peer review of this work.

Reprints and permissions information is available at www.nature.com/reprints.

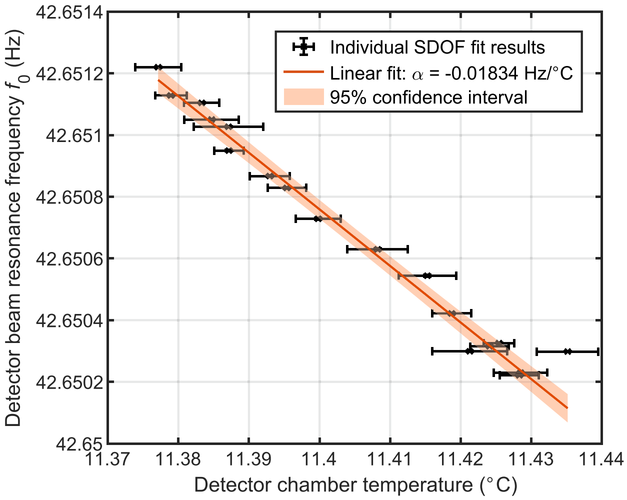

Extended Data Fig. 1 | Detector resonance frequency vs. temperature. Detector beam resonance frequency f_0 as a function of the mean temperature inside of the detector chamber. The points represent the SDOF fit result of the resonance frequency obtained from individual measurement runs (such as exemplarily shown in Fig. 3) at the mean temperature during the run (x - error bars = std). The y - error bars denote the 95% confidence interval of the SDOF fit result (not visible). The temperature of the air in the chamber and the beam's material are assumed to be equal. A linear fit of all data points reveals a linear relation between the detector resonance frequency and its temperature with a coefficient of −0.01834(56) Hz/°C. The red shaded illustrates the 95% confidence band of the linear fit.

Extended Data Table 1 | Detector and transmitter beam model parameters

Parameter	Unit	Transmitter beam		Detector beam	
		Value	**Standard uncertainty**	**Value**	**Standard uncertainty**
Mass	g	3875.6	0.1	647.72	0.02
Length	mm	1000.38	0.01	1000	0.01
Width	mm	10.05	0.01	8.49	0.01
Height	mm	20.07	0.01	16.97	0.01
Resonance frequency @ 11.4°C	Hz	42.58	0.01	42.650759	0.000015
Mass per unit length*	kg/m	3.8744	0.0001	0.6477	0.0002
Cross sectional area*	mm^2	201.7	0.2	144.1	0.2
Bending stiffness*	$\mathrm{Pa\,m}^4$	680.1	0.04	92.915	0.005
Young's modulus*	GPa	400	1	107.4	0.4
Second moment of inertia with respect to z-axis*	m^4	1.7E-09	5E-12	8.65E-10	3E-12

Dimensions and material properties of both transmitter and detector beam used for the analytical analysis of the gravitational coupling. The transmitter resonance frequency is influenced by the driving piezo and its backing mass. *Derived parameters using Euler-Bernoulli beam theory.